ChemComm

Graphitic Supramolecular Architectures Based On Corannulene, Fullerene, and Beyond

Journal:	*ChemComm*
Manuscript ID	CC-FEA-06-2021-002896.R1
Article Type:	Feature Article

ARTICLE

Graphitic Supramolecular Architectures Based On Corannulene, Fullerene, and Beyond

Gabrielle A. Leith[a] and Natalia B. Shustova[a*]

Received 00th January 20xx,
Accepted 00th January 20xx

DOI: 10.1039/x0xx00000x

In this Feature Article, we survey the advances made in the field of fulleretic materials over the last five years. Merging the intriguing characteristics of fulleretic molecules with hierarchical materials can lead to enhanced properties of the latter for applications in optoelectronic, biomaterial, and heterogeneous catalysis sectors. As there has been significant growth in the development of fullerene- and corannulene-containing materials, this article will focus on studies performed during the last five years exclusively, and highlight the recent trends in designing fulleretic compounds and understanding their properties, that has enriched the repertoire of carbon-rich functional materials.

Introduction

Over the past five years, there has been an influx of interest in expanding the realm of carbon-rich chemistry, with a focus on corannulene ($C_{20}H_{10}$, buckybowls) and fullerene (C_{60}, buckyballs) in particular (Fig. 1).[1–16] Significant advancements in the preparation of fullerene and corannulene (the smallest subunit of fullerene that retains its curvature) have been made since the advent of these new forms of carbon in 1985 and 1966, respectively.[17–21] Due to these synthetic improvements, the translation from their preparation in the laboratory to practical real-world applications became plausible. The curved structures of buckybowls and buckyballs endow the carbon architectures with interesting physicochemical, electrochemical, and electronic properties.[22–26] Due to the low-lying lowest unoccupied molecular orbital (LUMO) and unique curved surface, fullerenes and their derivatives have been used as electron-accepting units in a variety of applications ranging from supercapacitors and electrodes to drug delivery systems.[27–30] For instance, fullerene, C_{60}, can reversibly accept and stabilize up to six electrons on its surface, forming a stable hexaanion,[31,32] and therefore, could significantly affect the material electronic properties by promoting efficient charge and energy transfer (CT and ET, respectively).[31,32] However, one of the challenges in fullerene chemistry is that the synthesis of buckyballs and their derivatives relies on high performance liquid chromatography (HPLC) purification. At the same time, corannulene, $C_{20}H_{10}$, can be prepared in a traditional laboratory setting on a kilogram scale, without the involvement of labor-intensive chromatographic purification.[21] Similar to fullerene, corannulene can reversibly accept and stabilize up to four electrons on its surface, forming a stable tetraanion. The $C_{20}H_{10}$ molecule also possesses a significant dipole moment (2.1 D), while exhibiting tunable photophysical properties as a function of π-bowl derivatization.[23,33–35]

Overall, exploration of fulleretic assemblies has resulted in the discovery of larger buckybowl molecules,[36] design of nanographene-like materials,[5,17,36–41] and the formation of a carbon-based nanocone[42]. In addition to synthetic efforts, computational modelling has also predicted the formation of unique classes of innovative carbon structures,[43–45] provided strategies for enhancing nonlinear optical responses, and outlined routes for efficient intermolecular CT in carbon-based materials.[46,47] Due to a plethora of studies in the field of graphitic materials,[8,22,23,48,49] this Feature Article aims to shed light on the expansion of corannulene- and fullerene-based supramolecular motifs and extended architectures solely over the past five years. The main goal of this Feature Article is not to provide an all-inclusive review of fulleretic materials, but rather to highlight the most prominent trends and latest significant advances in the field.

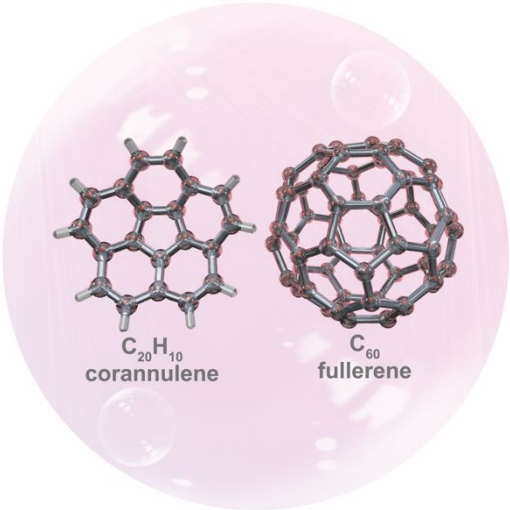

Fig. 1 Molecular structures of (*left*) corannulene, $C_{20}H_{10}$, and (*right*) fullerene, C_{60}.

[a] *Department of Chemistry and Biochemistry, University of South Carolina, Columbia, South Carolina 29208, USA*
Email: shustova@sc.edu
See DOI: 10.1039/x0xx00000x

Oligomers and Polymers

This section of the Feature Article will cover several advances in the field of corannulene- and fullerene-containing oligomers and polymers during the last five years. Notably, this section does not detail all discoveries in the corannulene- and fullerene-containing oligomer and polymer field, but instead brings attention to fundamental structural discoveries and harnessing the unique properties of fullerene- and corannulene-based materials. Comprehensive reviews published in the last few decades highlighting the properties of corannulene, fullerene, or buckybowl derivatives can be found elsewhere.[8,50–56]

In 2017, a family of discrete π-conjugated oligomers, containing corannulene (C) and thiophene (T) units connected with each other through an acetylene linkage, was reported by Stuparu and co-workers (Fig. 2).[57] The properties of the prepared oligomers, C_1T_1, C_2T_1, C_3T_2, and C_4T_3, were probed as a function of the oligomer length. As a result, a significant bathochromic shift in the oligomer absorption profile, upon increasing the chain length, was detected. For example, one of the main absorption bands in the spectrum of C_1T_1 possessed λ_{max} at 370 nm, while in the absorption spectrum of C_3T_2, λ_{max} was shifted to 450 nm.[57] The density functional theory (DFT) calculations corroborated the experimental results by demonstrating a decrease in the highest occupied molecular orbital (HOMO)-LUMO gap upon increasing the oligomer length. In addition, corannulene-containing oligomers with longer chains (e.g., C_3T_2) possessed a relatively high quantum yield of 40% (C_3T_2) in solution, a large two-photon absorption cross-section of 600 GM, and two-photon-excited bright luminescence, providing an avenue for further investigations of these materials for nonlinear optics applications.

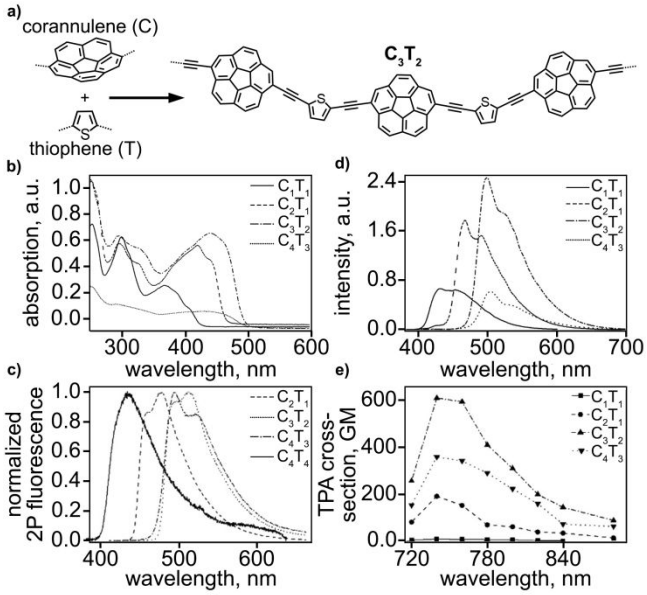

Fig. 2 (a) Schematic representation of C_3T_2 synthesis. (b) UV-vis absorption spectra of oligomers in chloroform (4×10^{-4} M). (c) Two-photon excited emission of oligomers in chloroform (4×10^{-4} M). (d) Emission spectra of oligomers in chloroform (4×10^{-4} M, λ_{ex} = 370 nm). (e) Two-photon action spectra of oligomers in chloroform. Reproduced from Ref. 57 with permission from the American Chemical Society.

The first examples of amorphous corannulene-based polymers were designed by the Smaldone group.[9] These materials were prepared through Sonogashira copolymerization of tetrabromocorannulene with monomers containing terminal alkyne groups such as 1,4-diethynylbenzene, 1,3,5-trisethynylbenzene, or tetra(4-ethynylphenyl)methane.[9] To probe the effect of π-bowl curvature on the possibility of gas adsorption, the authors examined the prepared corannulene-based materials for carbon dioxide uptake. The highest gas uptake measured for these polymers was found to be 57 $cm^3\ g^{-1}$ (11.7 wt%) at 273 K (and 900 mmHg), that is comparable (and even surpassed) the uptake of CO_2 observed by several porous organic materials such as COF-5 (7.4 wt%)[58], COF-103 (7.6 wt%)[58], or BLP-1H (7.4 wt%)[59].

In a similar vein, Stuparu and co-workers synthesized an amorphous polymer from a corannulene-based oxa-norbornadiene monomer using ring-opening metathesis polymerization.[60] This polymer possessed an average pore size of 1.4 nm and a surface area of 49 $m^2\ g^{-1}$. The prepared polymer also displayed a high specific capacitance value of 134 F g^{-1} at 0.5 A g^{-1} (1.0 V voltage window) measured in a three-electrode cell configuration. In the asymmetric supercapacitor, the prepared corannulene-based material was utilized as the positive electrode, while activated carbon was employed as the negative electrode. This corannulene-based supercapacitor displayed good cyclability with 90% capacitance retention after 10,000 cycles. Overall, this work was one of the first studies that outlined the previously proposed potential[3,9,27,28,61] of using corannulene-based polymers as electrochemical storage components. In line with these studies, it is important to mention Petrukhina's pioneering work focusing on tetrareduced corannulene bowls, $C_{20}H_{10}^{4-}$, with intercalated alkali metals.[62–65] In these studies, corannulene tetraanions were shown to self-assemble with multiple alkali metal cations into unique sandwich-type aggregates.[63] For instance, these investigations revealed the formation of triple-decker sandwiches containing high nuclearity $(Li_3M_3)^{6+}$ (M = K, Rb, and Cs) species between two tetrareduced corannulene decks.[63] Notably, two interior lithium ions within the $(Li_3M_3)^{6+}$ sandwiches could be replaced with larger alkali metals, resulting in $(LiM_5)^{6+}$ (M = K and Rb) motifs. However, the central lithium ion, trapped within the sandwich, stayed intact during the transmetallation procedure. Overall, these results could be used as a foundation for further understanding the lithium storage processes in carbonaceous materials.

Corannulene- and fullerene-containing nanomaterials have also been studied as potential candidates for biomedical applications.[30,66–68] For instance, a strategy developed by Tang and co-workers in 2018 led to the fabrication of corannulene-based aggregation-induced-emission (AIE) "dots" (Cor-AIE dots) for cancer phototheranostics (Fig. 3).[67] These corannulene-containing dots were constructed from 4-(2,2-bis(4-(diphenylamino)phenyl)-1-(4-methoxyphenyl)vinyl)-1-methylpyridinium hexafluorophosphate (TPP-TPA) and corannulene-decorated polyethylene glycol (Cor-PEG). For accurately comparing the properties, analogous DSPE-AIE dots

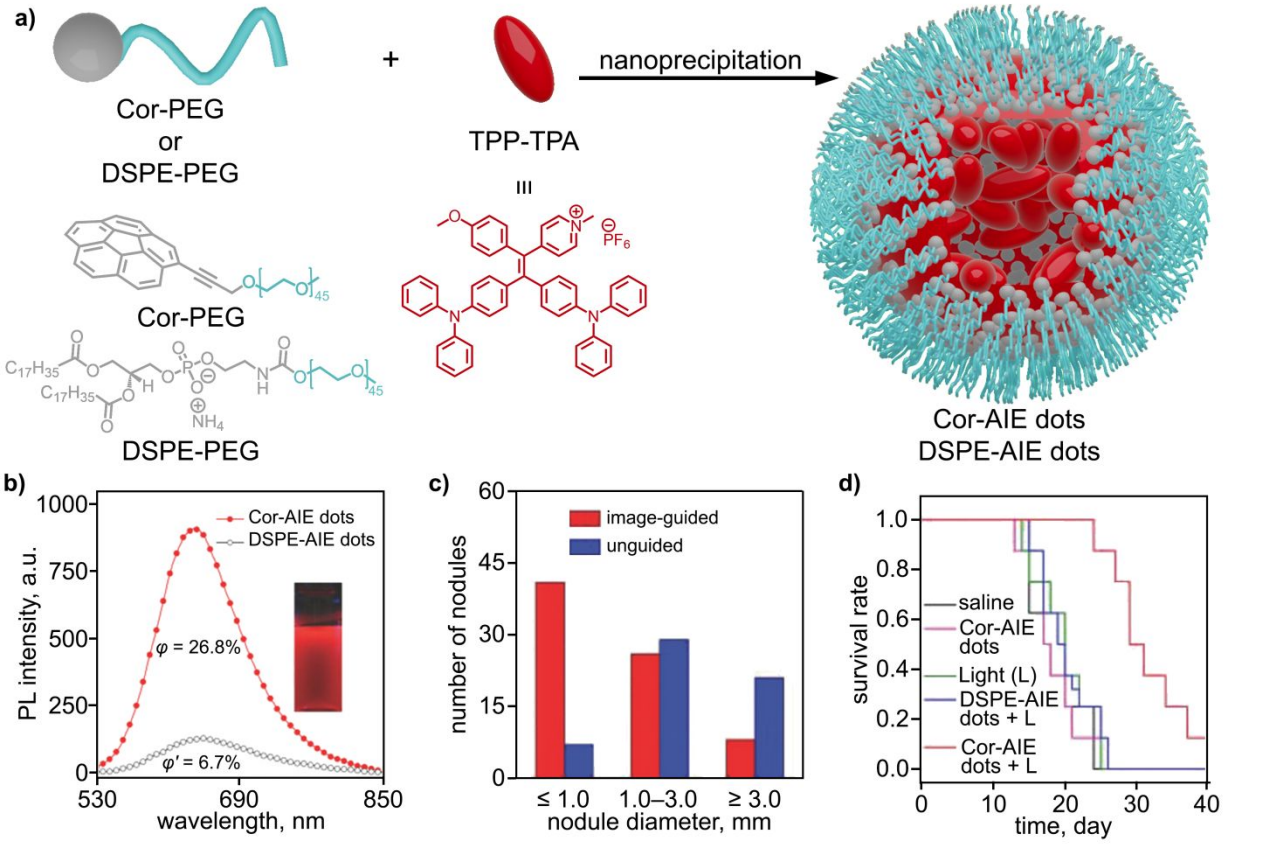

Fig. 3 (a) Schematic representation of the synthetic procedure used for Cor-AIE and DSPE-AIE dots. (b) Photoluminescence lifetime spectra collected for Cor-AIE and DSPE-AIE dots (λ_{ex} = 500 nm). Inset shows a photo of fluorescent Cor-AIE dots under λ_{ex} = 365 nm. (c) Histogram of nodule diameters extracted from unguided and Cor-AIE-guided groups. (d) The curve of mice survival rates after different treatments using "saline," "Cor-AIE dots," "light (L)," "DSPE-AIE dots + L," and "Cor-AIE dots + L." "L" indicates exposure under a white light (0.4 W cm^{-2}) for 10 minutes. Reproduced from Ref. 67 with permission from the Royal Society of Chemistry.

(without the inclusion of corannulene moieties) were constructed from the same linker, TPP-TPA, and 1,2-distearoyl-*sn*-glycero-3-phosphoethanolamine-*N*-[methoxy(polyethylene glycol)-2000] (DSPE-PEG). The following assessment of the two materials revealed that the Cor-AIE dots possessed a 4-fold greater fluorescence quantum yield and a 5.4-fold enhanced production of reactive oxygen species, in contrast to the DSPE-AIE dots. The authors hypothesized that the observed enhanced properties could be attributed to the presence of corannulene moieties in the dots. The corannulene molecules provided intraparticle rigidity and restricted intramolecular rotation of the TPP-TPA fragments, thus suppressing nonradiative decay pathways.[67] To demonstrate that the prepared fluorescent Cor-AIE material could be utilized for image-guided cancer surgery, mice with cancerous tissue were injected with the Cor-AIE dots. During *in vivo* NIR fluorescence studies, utilized for identification of the cancerous tissue during surgery, the Cor-AIE dots exhibited a very strong fluorescent response. After the Cor-AIE dot-guided surgery, 70% of the treated mice survived, while a 0% survival rate was reported for non-Cor-AIE-guided surgery. Thus, these results demonstrate the advantages and perspectives of employing fluorescent corannulene-based dots for *in vivo* NIR fluorescence image-guided surgery.

In 2021, Stuparu and co-workers investigated the formation of a biomedically relevant micellar structure possessing a corannulene-based fullerene-loaded core and a PEG shell (Fig. 4).[66] In these materials, the core is made up of a host polymer, containing corannulene moieties, that assembled with fullerenes due to the favorable interactions between concave and convex aromatic surfaces. As shown in Fig. 4, the host polymer block backbone has several corannulene moieties attached, allowing for structural accommodation of fullerenes of different sizes, such as C_{60} and C_{70}, in the micellar core. High fullerene loading was accomplished through the formation of micelles in the presence of fullerene, followed by polymer assembly and cross-linking to "lock in" the fullerene molecules, resulting in core-crosslinked nanoparticles (Fig. 4). This approach led to approximately 8 wt% of fullerene loading into the nanoparticles. Dynamic light scattering (DLS) studies were conducted to evaluate the micellar size and stability of the prepared nanoparticles. After cross-linking of the core, the micellar size was determined to be about 30 nm, and the prepared nanoparticles exhibited chemical stability at two measured pHs of 2.5 and 7.4 (Fig. 4).[66] Further investigations of "concave-convex" corannulene and fullerene assemblies could help to build a foundation for preparation of stable bionanomaterials for the detection and mediation of chronic or acute diseases.

Haino and co-workers recently explored a

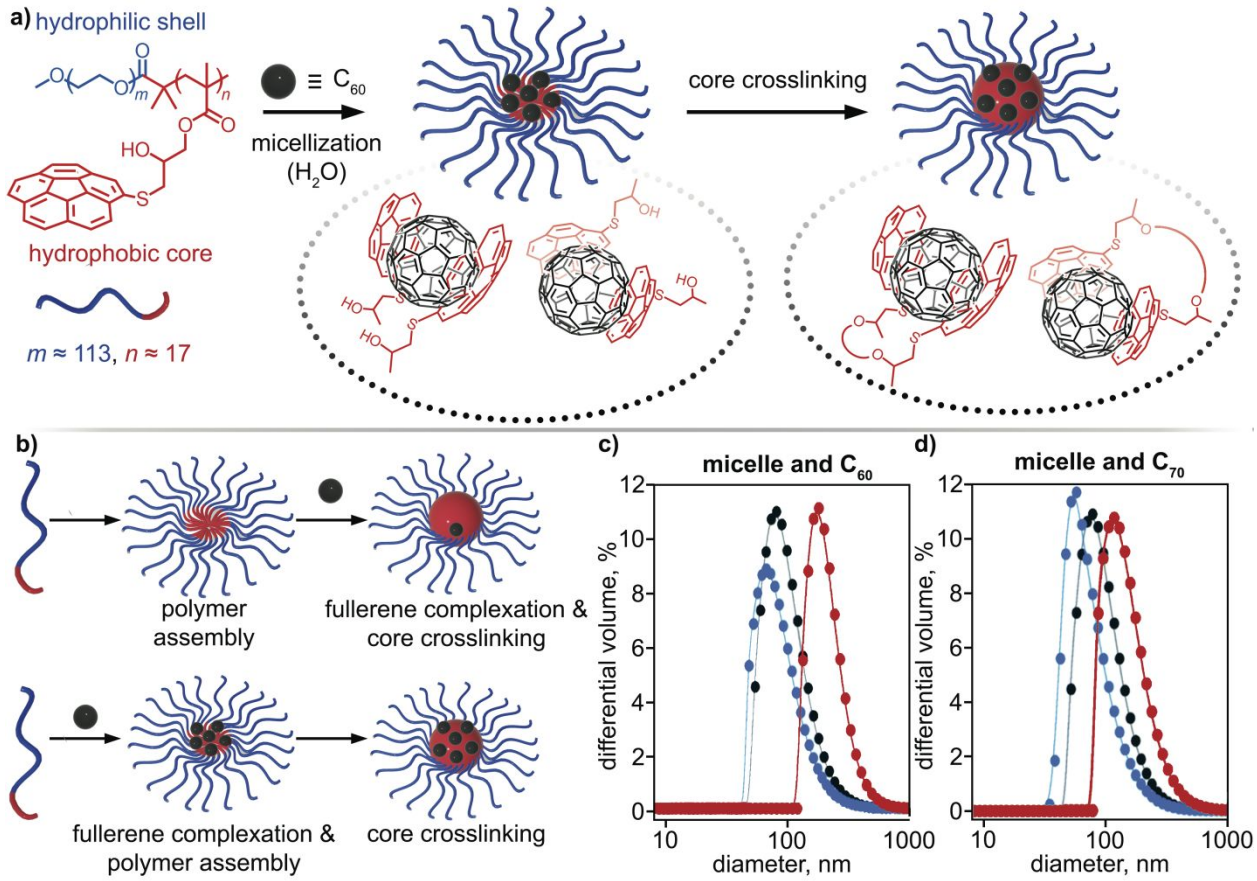

Fig. 4 (a) Chemical structure of host polymer with corannulenes and its assembly with fullerene through ball-and-socket interactions resulting in formation of micellar nanoparticles. (b) Two approaches for encapsulating fullerene into the host polymer micelle. (c) Dynamic light scattering (DLS) data for block copolymer micelles and C_{60} before cross-linking in water (black) and after cross-linking in water (blue) and after cross-linking in DMF (red). (d) DLS data for block copolymer micelles and C_{70} before cross-linking in water (black) and after cross-linking in water (blue) and after cross-linking in DMF (red). Reproduced from Ref. 66 with permission from the Royal Society of Chemistry.

supramolecular approach for merging fullerene and polymer areas.[69,70] In 2020, they created shape-transformable polymers based on calix[5]arenes, a macrocyclic molecule with a large cavity, that could bind fullerene-terminated polymethyl methacrylate (PMMA) via calixarene-fullerene complexation (Fig. 5).[69] The fullerene-terminated PMMA facilitated the formation of three unique shapes through assembling the macrocyclic host (linear ditopic, **2**, or branched tritopic, **3**) with fullerene-terminated PMMA in solution. Upon combining, the fullerene-terminated PMMA to either the linear ditopic or the branched tritopic calix[5]arene hosts, emission from the host was efficiently quenched. The authors hypothesized that the observed quenching occurred due to fullerene integration that is in line with previous literature reports.[71] The complexation of calixarene and fullerene was verified by size-exclusion chromatography and diffusion-ordered NMR spectroscopy.[69] To summarize, these results provided evidence that employing a supramolecular approach to shape-transformable polymers can allow for access to three distinct polymer shapes, and offers the foundation for fabricating stimuli-responsive fullerene-based materials.

In a follow-up study, the same group endeavored to create a main-chain fullerene-based polymer.[70] The authors achieved this through a helically-organized-fullerene array made by polymerizing a chiral ditopic tetrakiscalix[5]arene host with a dumbbell-shaped fullerene (Fig 6). The association between the chiral hosts and the fullerene molecules led to a sizable supramolecular polymer with a degree of polymerization exceeding 32. The prepared material was investigated by circular dichroism spectroscopy, and these studies demonstrated that the major transitions from 650 to 500 nm were associated with π–π^* fullerene derivative transitions. This successful design of the fullerene-containing polymer could be just the tip of the iceberg for the formation of new functional polymeric materials.

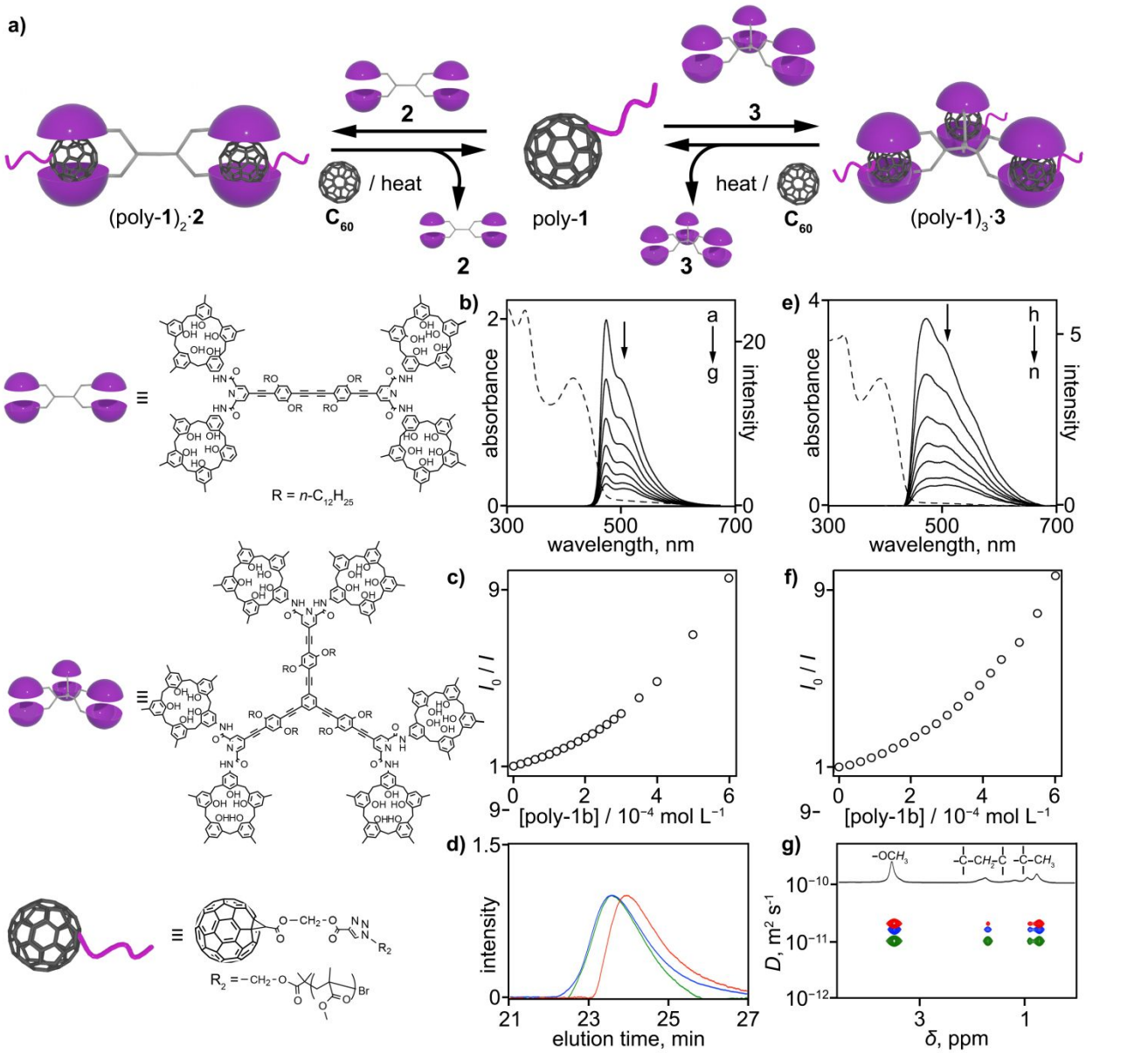

Fig. 5 (a) Schematic representation of polymer shape transformation by applying an external stimulus (e.g., heat). Changes in the fluorescence spectra of (b) **2** (1.0×10^{-4} mol L^{-1}, λ_{ex} = 420 nm) and (e) **3** (2.0×10^{-5} mol L^{-1}, λ_{ex} = 400 nm) upon the addition of poly-**1b**. The dashed line indicates the absorption spectrum of (b) **2** or (e) **3** (2.0×10^{-5} mol L^{-1}). Stern-Volmer plots for (c) **2** and (f) **3** in the presence of poly-**1c**. (d) Size-exclusion chromatogram of poly-**1b** (red line), a 1:2 mixture of poly-**1b** and **2** (blue line), and a 1:3 mixture of poly-**1b** and **3** (green line) in toluene. (g) Diffusion coefficients (*D*) of poly-**1b**, as inferred from diffusion-ordered NMR measurements in chloroform-*d*. The red, blue, and green lines denote the spectra obtained from poly-**1b**, a 2:1 mixture of poly-**1b** and **2**, and a 3:1 mixture of poly-**1b** and **3**, respectively. Reproduced from Ref. 69 with permission from the American Chemical Society.

The presented papers in the section of fullerene- and corannulene-based materials only provides a general overview on the progress made in the past five years in this community. Thus, several reports have harnessed the advantages of flexible polymer materials for manipulating and restricting fullerene molecules, whether that is within the polymer chain itself or with the assistance of a host. The applications of these materials are far-reaching, promoting advances in biomedical, gas adsorption, and stimuli-responsive material research areas.

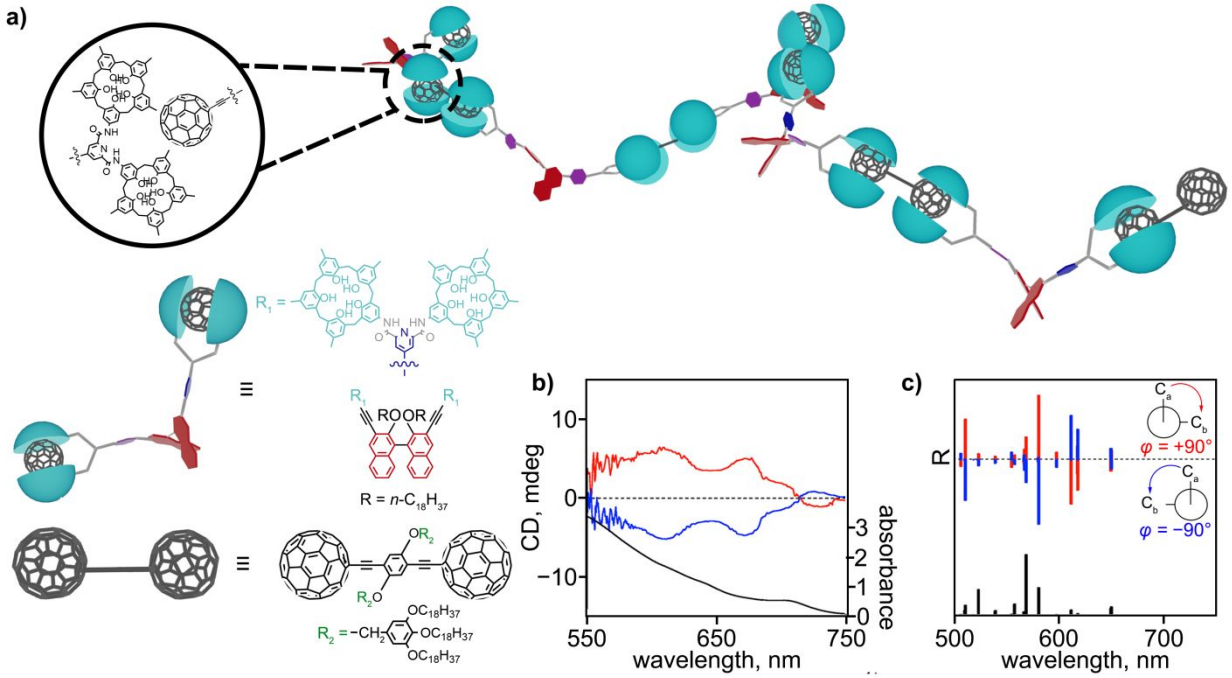

Fig. 6 (a) Molecular structures of tetrakiscalix[5]arene (teal), dumbbell-shaped fullerene (black), and the main-chain fullerene polymer. (b) Circular dichroism (CD) spectra of 1:1 mixture of (red) *R*-tetrakiscalix[5]arene (1.0×10^{-2} mol L^{-1}) and dumbbell-shaped fullerene (1.0×10^{-2} mol L^{-1}) and (blue) (*S*)-tetrakiscalix[5]arene (1.0×10^{-2} mol L^{-1}) and dumbbell-shaped fullerene (1.0×10^{-2} mol L^{-1}) at 278 K. The black line denotes the UV-vis absorption spectrum of a 1:1 mixture of (*R*)-tetrakiscalix[5]arene (1.0×10^{-2} mol L^{-1}) and dumbbell-shaped fullerene (1.0×10^{-2} mol L^{-1}) at 278 K. (b) Calculated CD and UV-vis absorption spectra of a model compound with a dihedral angle (φ)of ±90° Reproduced from Ref. 70 with permission from the American Chemical Society

Covalent-Organic Frameworks

Merging the properties of buckybowl and buckyball molecules with extended crystalline organic scaffolds such as covalent-organic frameworks (COFs) is an area that has only recently started to be explored. Several studies have demonstrated that two-dimensional (2D) COFs can be used as templates for controlling the structural arrangement of fulleretic guest molecules including corannulene and fullerenes, C_{60} or C_{70}.[72–75] For instance, Bein and co-authors designed the first COF-based fullerene-containing UV-to-NIR-responsive photodetector.[76] For that, [6,6]-phenyl C_{71} butyric acid methyl ester ($PC_{71}BM$) was spincoated onto a layer of COF that was deposited on a MoO_x surface of indium tin oxide-coated glass substrate. The resulting interdigitated heterojunction acted as the active layer in a voltage-switchable photodetector. At 0 mV bias, the photodetector displayed sensitivity toward blue and red light, while it did not exhibit any sensitivity toward green and NIR light. However, an increase in the reverse bias led to a decrease in the relative and absolute intensities in the blue and red spectral regions, and an increase in the green and NIR regions. Thus, nearly complete inversion of spectral sensitivity was achieved, providing a pathway forward for applications of these materials in the information technology or spectral imaging sectors.

The electronic properties of buckybowl- and buckyball-integrated COFs were probed by Shustova and co-workers over the last four years.[77,78] In 2018, the Shustova research group designed the first example of a donor-acceptor (D-A) COF in which the buckybowl was integrated through (i) coordinative immobilization using a copper-catalyzed azide-alkyne cycloaddition (CuAAC) and (ii) non-coordinative encapsulation.[77] The selected parent COF possesses a pore aperture of 33 Å, that was sufficient for integration of bulky corannulene derivatives (with a diameter of ~6.6 Å). According to time-resolved and steady-state spectroscopic studies, CT between corannulene units and the COF matrix was detected.[77] Changes in the electronic profile of the prepared corannulene-containing COFs were surveyed by estimating the optical band gaps and performing bulk conductivity measurements. A decrease in the optical band gaps from 2.24 eV (the parent COF) to ~1.94 eV (for corannulene-integrated COFs) was reported, that was in line with the results from the conductivity measurements. Indeed, four-orders-of-magnitude and seven-orders-of-magnitude conductivity enhancement were observed for the COF that contained corannulene guest molecules and the framework with coordinatively-incorporated corannulene moieties, respectively. CT rate as a function of mutual corannulene orientation was evaluated through application of the Marcus theory. Within this model, the authors reported that a shift from noncolumnar organization (e.g., as a guest) to a 1D stack of corannulene molecules (e.g., covalently tethered to the COF) could result in a *ca.* 42-fold increase in conductivity. In a follow-up report, Shustova and co-workers targeted incorporation of a bulkier fulleretic molecule, fullerene C_{60}, inside the same COF matrix.[78] In a similar way to the previous synthesis of corannulene-containing COF, they covalently

tethered the bulky fullerene building block to the decorated COF walls, allowing for promotion of D-A alignment. Due to this favorable interaction between donor (parent COF) and acceptor (fullerene moiety), a six-orders-of-magnitude conductivity enhancement in the fullerene-integrated COF versus the parent COF was detected. Due to the integration of redox-active building blocks, C_{60} derivatives, the authors were able to perform electrochemical studies. Their investigations demonstrated an unrevealed potential for the utilization of fullerene-containing COFs for the development of electroactive multidimensional crystalline materials.

The field of fulleretic COFs remains in its infancy with a plethora of investigations yet to take place. Although the work discussed in this section has laid a solid foundation for future efforts to build upon, the current reports are primarily dominated by acquiring fundamental knowledge and pursuing electronic property investigations. Currently, there is a wealth of knowledge to be uncovered regarding fulleretic COFs that will hopefully be revealed within the next decade.

Metal-Organic Frameworks

Historically, fullerene-containing materials, such as fullerene-based metal-organic frameworks (MOFs), are the more explored class of materials in comparison with their corannulene analogs, and especially over the past five years, the fulleretic MOF community has blossomed.[79–83] Rational synthetic design and innovative approaches have led to the development of controllable, tunable hierarchical structures, that were previously inaccessible.[23,71,81,83,84]

As mentioned before, fullerenes possess an arsenal of unique characteristics including their curved surface and excellent electron-accepting properties. In this regard, incorporation of electron-accepting fullerene into traditionally insulating matrices, such as MOFs, can allow for tailoring and enhancing their electronic properties. For instance, Espallargas and co-workers targeted fullerene encapsulation into the MUV-2 framework consisting of a [$Fe_3(\mu_3$-O)$(COO)_6$] secondary building unit connected by $TTFTB^{4-}$ ligands (H_4TTFTB = 4,4',4'',4'''-([2,2'-bi(1,3-dithiolylidene)]-4,4',5,5'-tetrayl)tetrabenzoic acid.[85] Specifically, the H_4TTFTB linkers were chosen due to the tetrathiafulvalene (TTF) core, a well-known electron donor. The appearance of a broad band from 450–800 nm in the absorption profile supported the possibility of intermolecular CT between C_{60} and TTF units, that was also corroborated by theoretical calculations. The experimental optical band gap was estimated to be 1.4 eV for C_{60}@MUV-2, and electrical conductivity measurements revealed a two-orders-of-magnitude enhancement (4.7×10^{-9} S cm^{-1}) compared to MUV-2 itself (3.7×10^{-11} S cm^{-1}).

Huang and co-workers probed simultaneous MOF growth and C_{60} encapsulation inside UiO-67 (UiO = University of Oslo), followed by coordination of palladium nanoparticles to C_{60}, through metal-π-interactions, for catalytic applications.[86] The prepared hybrid fullerene-containing MOF was then employed for tandem hydrogenation. In particular, the synthesis of secondary arylamines was chosen as a model reaction that required three steps: (1) nitroarene hydrogenation, (2) reductive amination of aldehydes, and (3) selective hydrogenation, resulting in the formation of secondary arylamines. Comparison of the catalytic activity of the prepared hybrid with a previously reported MOF-supported Pd catalyst[86] demonstrated that the former catalyst required shorter reaction times and milder synthetic conditions.

Carbon-rich molecules are typically hydrophobic, and thus their incorporation into a porous matrix may affect the materials behavior in aqueous environments. Falcaro and co-workers employed this strategy to improve the stability of γ-cyclodextrin MOFs (γ-CD-MOFs) utilized for drug delivery applications (Fig. 7).[87] Typically, γ-CD-MOFs disintegrate instantly upon interaction with an aqueous environment due to an externally hydrophilic structure. However, the internal cavity of the MOF is hydrophobic, allowing for the incorporation of hydrophobic guest molecules such as fullerenes. Immobilization of C_{60} within the MOF cavities led to improvement of the hydrophobic material properties and increased the overall MOFs water-resistance. Indeed, immersion of C_{60}@γ-CD-MOF in water revealed that the MOF was stable in an aqueous environment for up to 24 hours. This fact is remarkable considering that crystals of the unmodified γ-CD-MOF were immersed in water and completely degraded within a few seconds. To probe C_{60}@γ-CD-MOF as a drug delivery vehicle, an anticancer drug, doxorubicin (DOX), was loaded into the composite. Kinetics studies demonstrated a 49.2%, 78.5%, and 92.2% release of DOX molecules in a buffer solution after 3, 6, and 18 hours, respectively (Fig. 7).

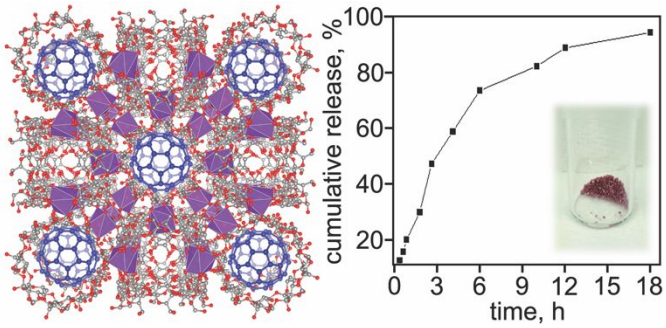

Fig. 7 (*left*) Schematic representation of the γ-CD-MOF/C_{60} composite. The purple polyhedra and gray and red spheres correspond to potassium, carbon, and oxygen atoms, respectively. Hydrogen atoms are omitted for clarity. Blue spheres represent C_{60} molecules. (*right*) Release profile of DOX@γ-CD-MOF/C_{60} at 37 °C. Reproduced from Ref. 87 with permission from the Royal Society of Chemistry.

During the past several decades, porphyrin-containing MOFs have attracted significant interest for fullerene encapsulation applications.[82,89–90] In the last five years, several research groups continued studying frameworks constructed from photoactive porphyrin building blocks and integrated fullerene molecules, targeting applications in the field of organic photovoltaics.[82,88,91] In 2016, the first example of a metal-organic fullerene-containing framework was reported, in which control over the mutual orientation of both donor and fullerene-based acceptor was achieved through coordination of fullerene-linkers to the metal.[71] To ensure mutual orientation of donor and acceptor molecules, a crucial aspect for active layer morphology

formation, the authors prepared electron-donating layers of Zn_2(ZnTCPP) (H_4TCPP = 5,10,15,20-tetrakis(4-carboxyphenyl)-porphyrin) and then installed the electron-accepting fullerene-based pillars, BPCF (BPCF = bis(pyridin-4-ylmethyl)-3'H-cyclopropa-[1,2](C_{60}-I_h)[5,6]fullerene-3',3'-dicarboxylate), forming the D-A Zn_2(ZnTCPP)$(BPCF)_{0.23}(DEF)_{0.77}$ framework (DEF = *N,N*-diethylformamide). DFT calculations were employed to gain a deeper understanding regarding the structural and electronic properties of Zn_2(ZnTCPP)$(BPCF)_{0.23}(DEF)_{0.77}$. Theoretical modeling demonstrated that the bands near the Fermi level had a small dispersion that was indicative of the frontier orbitals localized nature. The HOMO and LUMO orbitals in the *Γ*-point were found to be localized on ZnTCPP and BPCF, respectively. The photophysical behavior of the prepared fullerene-containing framework was significantly affected by the presence of fullerenes inside the MOF matrix. For instance, photoluminescence, originating from the Zn_2(ZnTCPP) layers, was nearly completely quenched upon fullerene integration. Time-resolved photoluminescence studies also demonstrated a significant decrease in the material lifetime values due to the installation of fullerene-based linkers. The estimated ET efficiency between porphyrin units and fullerene moieties was determined to be 49.5%, with a corresponding rate constant of 9.18×10^8 s^{-1}.[71]

In addition to empty buckyballs, encapsulation of endohedral metallofullerenes (containing metal or metal clusters inside the carbon cage) is of great interest due to their unique structures, magnetic behavior, and responsivity to a confined environment, i.e., displaying dramatically distinctive spin dynamics as a result of a confined space.[79,80,92] For instance, recent studies reported that incorporation of Gd@C_{82} into MOF-177 ($Zn_4O(BTB)_2$; H_3BTB = 1,3,5-benzenetribenzoic acid) led to pronounced magnetic behavior (Fig. 8).[79] In a 5–300 K temperature range, the magnetization-field strength (*M–H*) curve of Gd@C_{82}⊂MOF-177 indicated a paramagnetic pattern within the magnetic field near 0 tesla. Remarkably, the inverse magnetic susceptibility versus temperature (χ^{-1}–*T*) plot of Gd@C_{82}⊂MOF-177 revealed a transition from paramagnetic to antiferromagnetic behavior at *T* = 135 K. Although this work presented a new and unique magnetic host-guest system, developing magnetic extended architectures based on endohedral metallofullerenes is an area that is ripe with opportunity.

An example of a porous crystalline framework built from redox-active corannulene-based ligands, with the buckybowl derivatives covalently linked to zinc cations, was reported in 2016.[84] Coordinative immobilization of the corannulene linker allowed for maintenance of the bowl shape, in comparison with other literature reports demonstrating corannulene flattening owing to host-guest interactions.[93,94] The electrochemical studies revealed that the corannulene-based MOF had less negative reduction potentials, with values of ΔE_p(I) = −1.42 V and ΔE_p(II) = −1.69 V compared to pristine corannulene, ΔE_p(I) = −1.87 V and ΔE_p(II) = −2.41 V.[84] In the following year, Shustova and co-workers designed the first D-A corannulene-integrated MOF with efficient ligand-to-ligand ET.[81] The D-A alignment was achieved through the synthesis of the Zn_2(ZnTCPP) scaffold,

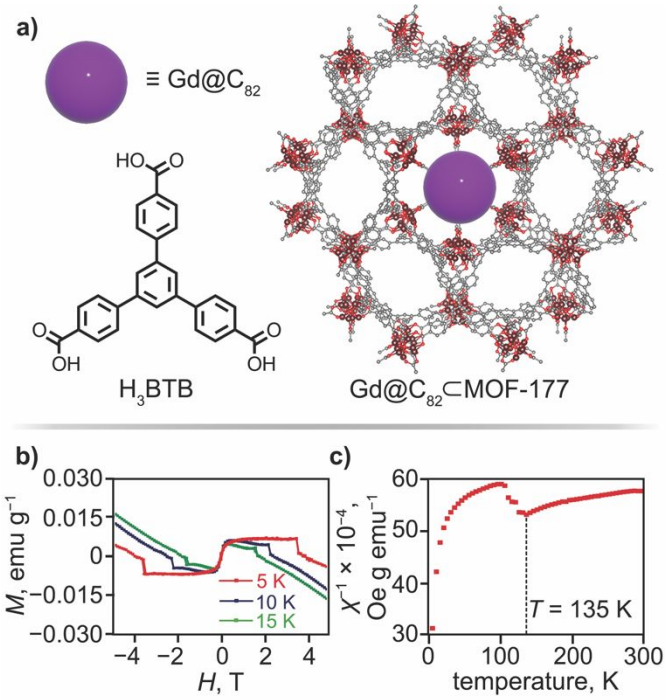

Fig. 8 (a) Single-crystal X-ray structure of MOF-177. The brown, gray, and red spheres correspond to zinc, carbon, and oxygen atoms, respectively. Hydrogen atoms are omitted for clarity. Purple sphere represents Gd@C_{82}. (b) *M–H* curve of Gd@C_{82}⊂MOF-177 measured at 5, 10 and 15 K. (c) χ^{-1}–*T* curve of Gd@C_{82}⊂MOF-177 measured between 5 and 300 K with an applied field of 0.1 T. Reproduced from Ref. 79 with permission from Taylor & Francis.

followed by corannulene-based pillar installation. As expected, based on the calculated spectral overlap function, incorporation of corannulene within the matrix led to nearly complete disappearance of the Zn_2(ZnTCPP) emission, that was indicative of efficient ET. Indeed, the ET efficiency was estimated to be 85% with an ET rate of 1.01×10^{-9} s^{-1}. This study was the first report describing the photophysics of any corannulene-based compounds in the solid state, and also presented the possibility to strategically engineer D-A corannulene-containing materials.

A recent study pursued preparation of a corannulene-containing MOF with integrated Pd nanoparticles for utilization in heterogeneous catalysis.[95] The support was constructed from ZIF-67 (ZIF = zeolitic imidazolate framework), containing corannulene as a guest, followed by electrochemical deposition of Pd nanoparticles on the framework surface. The resulting material demonstrated long-term stability under continuous CV cycles (up to 350) that were performed in a 1.0 M KOH solution containing 1.0 M methanol. Moreover, this composite possessed a large electrochemical surface area of 114.6 m^2 g^{-1} with a high electrocatalytic activity of 90.2 mA cm^{-2}.

Supramolecular Cages and Macrocycles

In the past five years, studies in the field of corannulene- and fullerene-based discrete supramolecular structures focused on initially gaining fundamental understanding of material properties, followed by considering their potential applications.[35,94,96–100] The field of discrete supramolecular motifs containing fullerene and corannulene has been cultivated over the years; therefore, the selected works in this section only provides a

glimpse of the progress made over the last five years. Reviews focusing on the integration of fullerenes in D-A arrays can be found elsewhere.[101–103] For example, a recently-reported corannulene-based coordination cage possessed a unique supramolecular helical structure existing as four stereoisomers; formation of the structure was attributed to bowl-to-bowl inversion.[104] The inherent chirality of the corannulene ligand, due to its concave shape,[105] could potentially be harnessed for chiral molecular recognition. Another unique corannulene-containing structure was reported by Jiang and co-workers, who prepared a self-assembled carcerand-like corannulene-based cage.[96] Due to the possibility of concave-convex interactions, the prepared cage served as a host for quantitative encapsulation of both C_{60} and C_{70}, and the prepared fullerene@cage possessed a relatively high thermal stability of 130 °C for 3 days. Due to temperature-dependent binding preference for C_{60} over C_{70} (C_{60} displaced C_{70} nearly quantitatively at 130 °C for 48 hours), this cage could also be used for purification and separation of C_{60} from C_{70} that originated from fullerene soot. The authors demonstrated the recyclability (up to five cycles) of the organic ligand (1,3,5,7,9-pentakis(3-pyridylethynyl)corannulene), used for the synthesis of the empty cage, after fullerene separation (necessary for regeneration of the Pd-based cage). Using a similar concept of fullerene separation (C_{60} from higher-order fullerenes, C_{2n} where $n \geq 35$), Gong and co-workers developed a macrocycle, CDMB-8 (CDMB-8 = cyclo[8](1,3-(4,6-dimethyl)benzene); Fig. 9).[106] The as-synthesized CDMB-8 macrocycle, possessing C_s symmetry, did not behave as an efficient fullerene receptor in the as-synthesized form. However, heating the macrocycle under anaerobic conditions at 300 °C for one hour resulted in an hourglass-like transformation, leading to symmetry changes from C_s to D_{4d} Fig. 9). In contrast to the as-synthesized material, the macrocycle (D_{4d}) obtained after heating could form complexes with both fullerenes, C_{60} and C_{70}, and more importantly, could separate C_{60} from C_{70}. To demonstrate the feasibility of the separation procedure, a mixture of CDMB-8, C_{60}, and C_{70} was dissolved in tetrachloroethane and allowed to precipitate over 48 hours. The precipitate revealed a C_{60}/C_{70} molar ratio of 9:91, according to HPLC analysis. Recrystallization

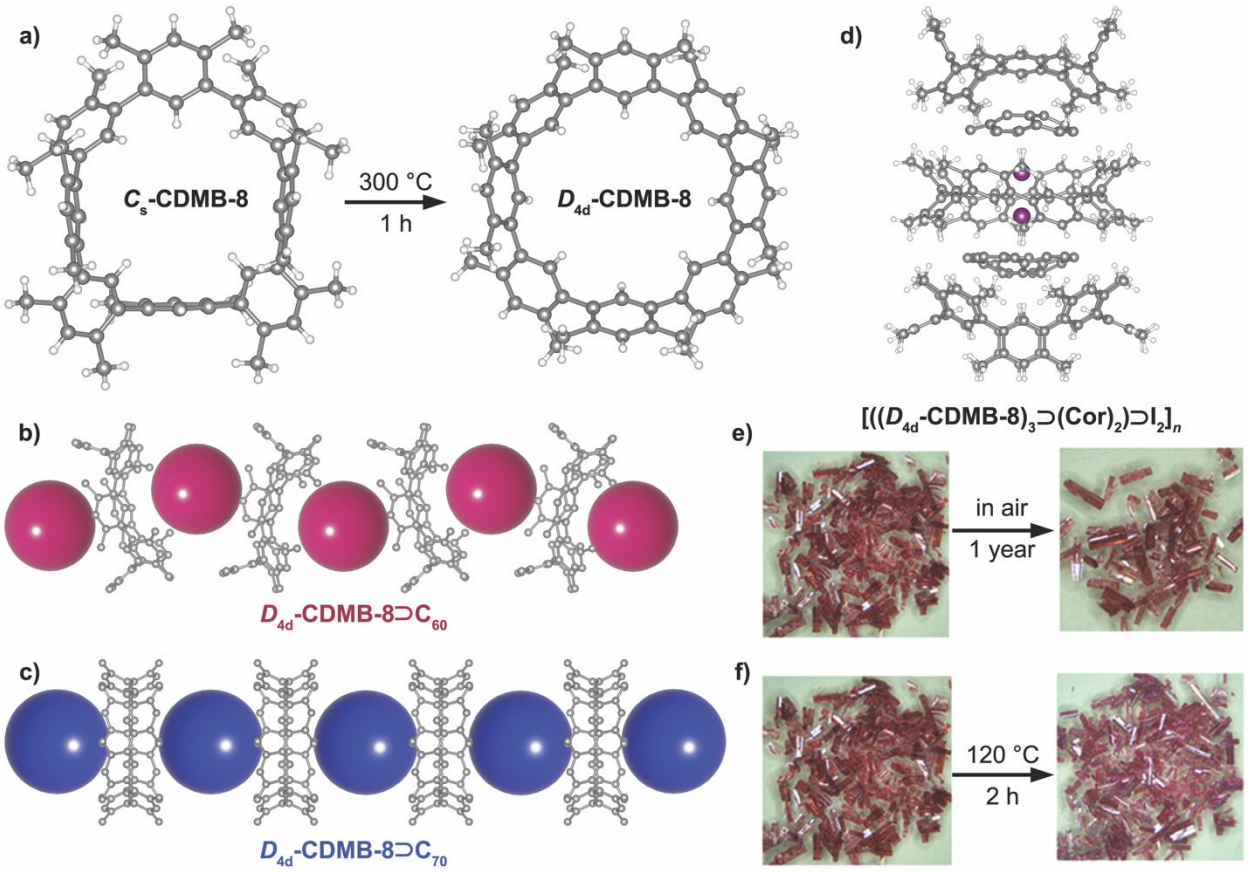

Fig. 9 (a) Single-crystal X-ray structure of C_s-CDMB-8 and D_{4d}-CDMB-8. The gray and white spheres correspond to carbon and hydrogen atoms, respectively. (b) Single-crystal X-ray structure showing interactions between D_{4d}-CDMB-8⊃C_{60}. The gray spheres correspond to carbon. Hydrogen atoms are omitted for clarity. The pink spheres correspond to C_{60} molecules. (c) Single-crystal X-ray structure showing interactions between D_{4d}-CDMB-8⊃C_{70}. The gray spheres correspond to carbon atoms. Hydrogen atoms are omitted for clarity. The blue spheres correspond to C_{70} molecules. Reproduced from Ref. 106 with permission from the Royal Society of Chemistry. (d) Single-crystal X-ray structure of the iodine-containing capsule, (D_{4d}-CDMB-8)$_3$⊃(Cor)$_2$⊃I_2. The purple, gray, and white spheres correspond to iodine, carbon, and hydrogen atoms, respectively. (e) Photographs of single crystals of (D_{4d}-CDMB-8)$_3$⊃(Cor)$_2$⊃I_2 as prepared and after exposure to air for 1 year at room temperature. (f) Photographs of single crystals of (D_{4d}-CDMB-8)$_3$⊃(Cor)$_2$⊃I_2 as prepared and after heating at 120 °C for 2 hours. Reproduced from Ref. 98 with permission from the American Chemical Society.

of the precipitate led to an enhanced molar ratio for C_{60}/C_{70} of <1:99 with a molar yield of C_{70} of 43%. A similar experiment was performed for separation of C_{60} from a mixture of higher fullerenes, C_{2n} where $n \geq 35$, resulting in a purity of C_{60} above 99% and a 35% mass yield.[106] These results demonstrate an alternative pathway for separation and purification of C_{60} and higher fullerenes in comparison with the traditional HPLC approach.

In a follow-up study, Gong and co-workers utilized the same CDMB-8 to probe the formation of a capsule-like ensemble with corannulene, and its utilization for capturing volatile guest molecules.[98] As shown in Fig. 9, a stack of alternating macrocycle (3 units) and corannulene molecules (2 units) efficiently trapped an iodine molecule, forming a supramolecular assembly, $[(CDMB\text{-}8)_3 \supset (Cor)_2) \supset I_2]_n$. Further examination of the I_2@complex properties revealed that iodine sublimation from the confined environment of the supramolecular structure was hindered, even at 145 °C. Furthermore, the I_2@complex crystals were stable in air for one year, and the same crystals maintained their integrity even upon heating at 120 °C for two hours (Fig. 9).[98] Thus, the corannulene-containing supramolecular assembly could efficiently trap a guest molecule and exhibited unique thermostability without releasing highly-volatile species.

Along with these studies, a 2019 report highlighted the versatility of a chiral and flexible decapyrrylcorannulene host that could entrap and align a significant number of different fullerenes (e.g., 15 different cages were tackled) that resulted in the crystallographic resolution of various molecular structures of previously unknown fullerene cages.[99] The concave corannulene core was decorated with electron-rich pyrryl moieties to mimic molecular "hands" for cradling a number of buckyballs in a (+)hand-ball-hand(-) mode (each pair of chiral molecules is indicated by (+) and (-)). This design is similar to the well-known "buckycatcher" host[107–109] that provided evidence of concave-convex π-π interactions.[107] In addition, these molecular tweezers can also assist in reducing crystallographic disorder, allowing for the precise identification of novel fullerene structures through single-crystal X-ray diffraction.[100,110–112] Furthermore, decapyrrylcorannulene could host nearly all of the currently known types of fullerenes including exohedral, endohedral, dimeric, fulleroid, pentagon-fused, and heteroderivatized structures, and participated in the assembly of 2D layered structures.[99]

In a similar vein to the decapyrrylcorannulene host, Maeda and co-workers synthesized curved π-electronic molecules, dipyrrolylbenzodiazepine derivatives, that could assemble with C_{60} (Fig. 10).[113] Specifically, dipyrrolylbenzodiazepines were synthesized as seven-membered heterocycle-based dipyrrolyl derivatives that co-assembled with C_{60}, resulting in the formation of a D-A system. Crystallographic packing revealed that dipyrrolylbenzodiazepines formed a hydrogen-bonding 1D chain structure with bonding between the pyrrole NH group and the diazepine nitrogen atom (Fig. 10), resulting in an unusual complex in which C_{60} was surrounded by a ring made from the

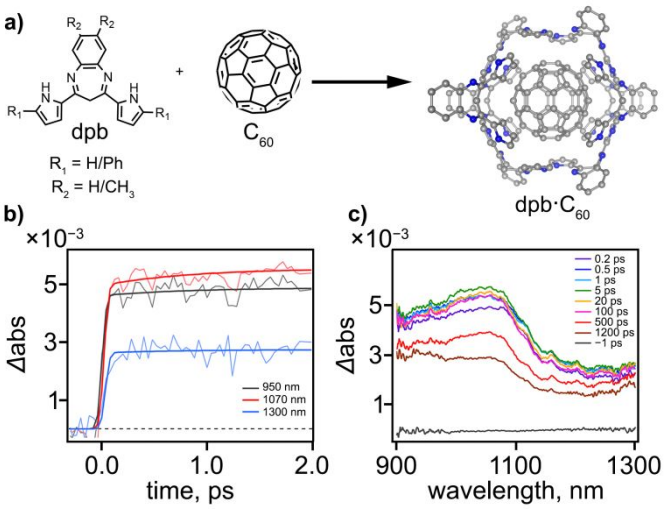

Fig. 10 Molecular structures of dipyrrolylbenzodiazepine derivatives and fullerene forming donor-acceptor (D-A) structures. Single-crystal X-ray structure of the D-A cocrystals. The gray and blue spheres correspond to carbon and nitrogen atoms, respectively. (b) Transient absorption decay profiles of the material in the ranges from −0.3 to 2 ps excited at 400 nm and monitored at 950 (black), 1070 (red), and 1300 nm (blue). (c) Subpicosecond to nanosecond transient absorption spectra of a single crystal excited at 400 nm with delay time spanning from −1 to 1200 ps. Reproduced from Ref. 113 with permission from the American Chemical Society.

assembled dipyrrolylbenzodiazepines. The same group probed the possibility of electron transfer in their D-A cocrystals by utilizing transient absorption (TA) spectroscopy in the near-infrared light region. Excitation of the donor (dipyrrolylbenzodiazepine) was performed by utilizing a 400 nm excitation wavelength, resulting in the appearance of a broad absorption band near 1070 nm. The authors attributed this band to the formation of a C_{60} radical anion. The estimated electron transfer in this system occurred in less than the tens of femtosecond range, that is notably faster than that observed in other donor-C_{60} systems in which the typical reported electron transfer occurred within hundreds of femtoseconds or picoseconds.[114,115] Based on experimental evidence and time-dependent density functional theory (TD-DFT) calculations, the authors hypothesized that the observed ultrafast electron transfer occurred due to the close proximity of the donor and acceptor arising from the curved geometry of the donor. Notably, the TA measurements also suggested that the photogenerated carriers could be transported over several D-A units along the *c*-axis, portending the potential of the crystals as 1D photoconductive materials.

Another example of investigating CT interactions in a fullerene-based supramolecular cocrystal was performed by Kim and co-workers in 2020.[116] They utilized a shape-persistent zinc-metalated porphyrin box (Zn-PB) and C_{60}/C_{70} to construct the porphyrin/fullerene cocrystals. This was the first example of fullerene tetramers that were prepared and in close proximity to one another. Notably, the fullerene tetramers were surrounded by six Zn-PBs forming D-A domains. The C_{60} tetramers and Zn-PBs close packing arrangement (with a distance of 3.1 Å between Zn and C_{60}) promoted CT. Spectroscopic investigations revealed the formation of charge-separated states with long lifetimes in the excited state and a

remarkably high photoconductivity compared to that of crystalline Zn-PB (a 10-fold enhancement in transient photoconductivity was observed for Zn-PB/4C_{60} that had a value of 3.1 × 10^{-5} cm^2 v^{-1} s^{-1}). Similarly, a 3-fold enhancement in transient photoconductivity was observed for Zn-PB/4C_{70}.[116]

In a similar vein, Beuerle and co-workers utilized a trigonal-bipyramidal covalent organic cage as a host for complexation of C_{60} and C_{70}.[117] In contrast to the previous reports focused on the electronic properties of D-A dyads, the authors endeavored to utilize the cage as a template to functionalize C_{60}. Based on UV-vis titration experiments, 1:1 complexes of cage⊃C_{60} and cage⊃C_{70} had binding constants of (6.3 ± 0.4) × 10^5 and (5.3 ± 0.4) × 10^5 M^{-1}, respectively. According to crystallographic analysis, only four *trans*-trisadducts formed due to matching the trigonal planar arrangement of the cage windows, allowing for selective exohedral functionalization of C_{60}. The authors performed a Prato reaction for C_{60}-integrated inside the cage and formed a symmetry-matched trisadduct of C_{60}, that typically only forms in trace amounts without the presence of a cage. These findings present another route to realize regioselectivity in a Prato reaction that is intrinsically nonselective, paving the way for the application of covalent-organic cages as templating agents for functionalizing complex π-systems.

Several noteworthy structures containing corannulene were also formed in the past five years and analyzed crystallographically. The Nitschke group probed the reaction of *sym*-pentakis(4-aminothiophenyl)corannulene with different organic linkers (e.g., 2-formyl-6-methylpyridine and 2-formyl-1,10-phenanthroline) and metals (e.g., copper, cobalt, and zinc).[118] Their efforts led to the formation of two unique structures: the first was an S_{10} symmetric five-fold interlocked [2]catenane, while the second cage possessed D_5 symmetry.[118] According to DFT calculations, the driving force for the formation of the [2]catenane interlocked structure was aromatic stacking interactions. Notably, another driving force highlighted in a recent report,[35] that could play a crucial role in the discovery of novel corannulene-based derivatives and could promote extraordinary structural transformation, is strain energy.[35] The Shustova group recently described an unprecedented C=C bond cleavage of pristine corannulene in a one-pot solid-state reaction, forming a planar corannulene analog, $C_{20}H_{14}$.[35] The reported approach could open an avenue for preparation of highly complex structures that are not accessible through conventional routes, and therefore, could advance applications in the areas of field-effect transistors, light-emitting diodes, or conductive electrodes.

The field of supramolecular cages and macrocycles has grown leaps and bounds over the past five years. Innovative approaches fusing molecular dynamics simulations with 2D NMR spectroscopy, as portrayed, for instance, by Ribas and co-workers, has led to a greater understanding of the nuances directing encapsulation.[119] Similarly, the advantages of utilizing a confined space, e.g., a cage or macrocycle, to restrict curved molecules has led to rapid energy and charge transfer as well as synthetic feats that were previously challenging.[98,117,118]

Conclusion and Outlook

As highlighted in this report, interest in the design and preparation of fulleretic materials is unrelenting. Several extraordinary structures containing corannulene and fullerene building units have recently been created. Moreover, tailoring the properties of MOFs and COFs, a rapidly growing research field, through integration of buckybowls and buckyballs has been put in motion.[71,78,81,84] Despite very few reports that currently exist in the area of fulleretic frameworks, D-A alignment facilitated through coordinative immobilization of curved molecules as linkers within a rigid matrix, or through non-coordinative inclusion of buckybowls(ball) as guests inside the pores, could significantly affect the photophysics and electronic properties of the resulting materials.[71,78,81,84] Furthermore, extensive studies of corannulene and alkali metal interactions performed by Petrukhina's research team provided an intriguing guiding hand for merging the intrinsically high surface area of COFs or MOFs with the high reversible alkali metal capacity inherent to corannulene and its derivatives.[62–65] Currently, literature reports in this direction are primarily dominated by supramolecular discrete structures, that could be used to provide valuable insight and design principles for extended structure engineering.

Fullerene, and especially its derivatives such as PCBM, have been extensively explored in the field of organic photovoltaics over the last few decades, while the corannulene family has not received much attention for applications in this direction.[120–125] However, the first attempts in this avenue demonstrated that corannulene derivatives (a naphthalimide-annulated corannulene) could be used as an electron acceptor, and in combination with an electron-donating polymer (PCE-10), resulted in a power conversion efficiency (PCE) of 2.1%.[126]

Another recent trend for improving the performance of photovoltaics is the addition of curved molecules for enhancement of the materials hydrophobicity (e.g., the perovskite layer).[122] For instance, one study reported the incorporation of corannulene-pentakis-(triethyleneglycol-monomethyl ether)-sulfone (Cor-TEG), containing a hydrophobic corannulene core and hydrophilic side chains, for increasing the moisture resistivity of a perovskite solar cell device.[122] This strategic design resulted in a noteworthy PCE of 17%, that only changed slightly (15.4%) after 65 days under inert conditions or under a humid environment (14.8%).[122] One rationale for the observed high PCE was attributed to the enhanced charge carrier mobility due to the electron-withdrawing nature of the corannulene derivative.

The first steps in the arena of corannulene-based biomaterials were only recently taken and already demonstrated corannulene's potential for applications in image-guided surgery for the successful removal of cancerous tissue.

To summarize, the field of fulleretic architectures has achieved extraordinary feats over the past five years in a number of areas mentioned above, including recent discoveries in the rapidly growing fields of metal- and covalent-organic frameworks. The possibility of merging the advantages of

hierarchical crystalline structures (COFs and MOFs) with buckybowls(balls) possessing unique electronic properties, dipole moments, spin dynamics (for endohedral metallofullerenes), and 3D curved surfaces, could portend the discovery of novel applications that are thus far unrealized.

Conflicts of interest

There are no conflicts to declare.

Acknowledgements

N. B. S. is grateful for support from an NSF CAREER Award (DMR-1553634) and NSF Award (DMR-2103722). N. B. S. also acknowledges support from the Cottrell Scholar Award from the Research Corporation for Science Advancement, the Dreyfus Teaching-Scholar Award supported by the Dreyfus Foundation, and the IAS Hans Fischer fellowship.

Biographies

G. A. Leith is currently pursuing her Ph.D. degree in organic chemistry at the University of South Carolina after completing her B.A. degree in chemistry from Hanover College in 2017. Her research focuses on designing donor-acceptor graphitic supramolecular architectures to promote directional charge transfer in a predesigned pathway.

N. B. Shustova is a McCausland Professor of chemistry at the University of South Carolina and a Hans Fischer Fellow. She received her M.S. degree in materials science from Moscow State University (MSU), Russia, and Ph.D. degrees in physical and inorganic chemistry from MSU and Colorado State University, respectively. She completed postdoctoral training at the Massachusetts Institute of Technology. Her research interests include graphitic hybrid materials for sustainable energy conversion, artificial biomimetic systems, actinide chemistry, and stimuli-responsive materials. Her research accolades include the IAS Hans Fischer and Alfred P. Sloan Fellowships and Camille Dreyfus Teaching-Scholar, Cottrell Scholar, and NSF Career and Breakthrough Awards.

Notes and References

1 R. K. Radha Krishnan, B. J. Reeves, S. H. Strauss, O. V. Boltalina and B. Lüssem, *Org. Electron.*, 2020, **86**, 105898.
2 C. Dubceac, Y. Sevryugina, I. V. Kuvychko, O. V. Boltalina, S. H. Strauss and M. A. Petrukhina, *Cryst. Growth Des.*, 2018, **18**, 307–311.
3 M. Gaboardi, F. Pratt, C. Milanese, J. Taylor, J. Siegel and F. Fernandez-Alonso, *Carbon N. Y.*, 2019, **155**, 432–437.
4 X. Tian, L. M. Roch, N. Vanthuyne, J. Xu, K. K. Baldridge and J. S. Siegel, *Org. Lett.*, 2019, **21**, 3510–3513.
5 C. Bruno, E. Ussano, G. Barucca, D. Vanossi, G. Valenti, E. A. Jackson, A. Goldoni, L. Litti, S. Fermani, L. Pasquali, M. Meneghetti, C. Fontanesi, L. T. Scott, F. Paolucci and M. Marcaccio, *Chem. Sci.*, 2021, **12**, 8048–8057.
6 A. Y. Rogachev, Y. Zhu, Z. Zhou, S. Liu, Z. Wei and M. A. Petrukhina, *Org. Chem. Front.*, 2020, **7**, 3591–3598.
7 Z. Zhou, Z. Wei, Y. Tokimaru, S. Ito, K. Nozaki and M. A. Petrukhina, *Angew. Chem. Int. Ed.*, 2019, **58**, 12107–12111.
8 E. Nestoros and M. C. Stuparu, *Chem. Commun.*, 2018, **54**, 6503–6519.
9 A. A. K. Karunathilake, C. M. Thompson, S. Perananthan, J. P. Ferraris and R. A. Smaldone, *Chem. Commun.*, 2016, **52**, 12881–12884.
10 H. T. Mitchell, M. K. Smith, N. D. Blelloch, D. W. Van Citters and K. A. Mirica, *Chem. Mater.*, 2017, **29**, 2788–2793.
11 Y. Wang, X. Chen, Q. G. Zhai, J. Guo and P. Feng, *J. Power Sources*, 2019, **434**, 126678.
12 I. I. Stoikov, D. S. Ibragimova, N. V. Shestakova, D. B. Krivolapov, I. A. Litvinov, I. S. Antipin, A. I. Konovalov and I. Zharov, *Supramol. Chem.*, 2009, **21**, 564–571.
13 Y. Zhang, Y. Zhu, D. Lan, S. H. Pun, Z. Zhou, Z. Wei, Y. Wang, H. K. Lee, C. Lin, J. Wang, M. A. Petrukhina, Q. Li and Q. Miao, *J. Am. Chem. Soc.*, 2021, **143**, 5231–5238.
14 J. E. Huang, D. J. Guo, Y. G. Yao and H. L. Li, *J. Electroanal. Chem.*, 2005, **577**, 93–97.
15 J. L. Shott, M. B. Freeman, N. A. Saleh, D. S. Jones, D. W. Paley and C. Bejger, *Inorg. Chem.*, 2017, **56**, 10984–10990.
16 X. Tian, J. Xu, K. K. Baldridge and J. S. Siegel, *Angew. Chem. Int. Ed.*, 2020, **59**, 1460–1464.
17 G. Báti, D. Csókás, T. Yong, S. M. Tam, R. R. S. Shi, R. D. Webster, I. Pápai, F. García and M. C. Stuparu, *Angew. Chem. Int. Ed.*, 2020, **59**, 21620–21626.
18 W.-B. Zhang, J. He, X. Dong, C.-L. Wang, H. Li, F. Teng, X. Li, C. Wesdemiotis, R. P. Quirk and S. Z. D. Cheng, *Polymer*, 2011, **52**, 4221–4226.
19 J. P. Barham, S. Tanaka, E. Koyama, N. Ohneda, T. Okamoto, H. Odajima, J.-I. Sugiyama and Y. Norikane, *J. Org. Chem.*, 2018, **83**, 4348–4354.
20 H. Keypour, M. Noroozi and A. Rashidi, *J. Nanostructure Chem.*, 2013, **3**, 45–53.
21 A. M. Butterfield, B. Gilomen and J. S. Siegel, *Org. Process Res. Dev.*, 2012, **16**, 664–676.
22 R. Chen, R.-Q. Lu, P.-C. Shi and X.-Y. Cao, *Chinese Chem. Lett.*, 2016, **27**, 1175–1183.
23 A. M. Rice, E. A. Dolgopolova and N. B. Shustova, *Chem. Mater.*, 2017, **29**, 7054–7061.
24 J. Yadav, *Res. Rev. J. Phys.*, 2017, **6**, 1–6.
25 Z. Biglari and H. Rezaei, *Comput. Theor. Chem.*, 2020, **1190**, 113002.
26 R. Macovez, *Front. Mater.*, 2018, **4**, 46.
27 B. A. Ali, A. H. Biby and N. K. Allam, *ChemElectroChem*, 2020, **7**, 1672–1678.
28 A. J. Khan, M. Hanif, M. S. Javed, S. Hussain and Z. Liu, *J. Mater. Sci. Mater. Electron.*, 2019, **30**, 8568–8576.
29 H. Kazemzadeh and M. Mozafari, *Drug Discov. Today*, 2019, **24**, 898–905.
30 M. Kumar and K. Raza, *Pharm. Nanotechnol.*, 2017, **5**, 169–179.
31 W. E. Billups and M. A. Ciufolini, *Buckminsterfullerenes*, VCH, New York, 1993.
32 Y.-T. Wu and J. S. Siegel, *Chem. Rev.*, 2006, **106**, 4843–4867.
33 G. Valenti, C. Bruno, S. Rapino, A. Fiorani, E. A. Jackson, L. T. Scott, F. Paolucci and M. Marcaccio, *J. Phys. Chem. C*, 2010, **114**, 19467–19472.
34 J. Mack, P. Vogel, D. Jones, N. Kaval and A. Sutton, *Org. Biomol. Chem.*, 2007, **5**, 2448–2452.
35 G. A. Leith, A. M. Rice, B. J. Yarbrough, P. Kittikhunnatham, A. Mathur, N. A. Morris, M. J. Francis, A. A. Berseneva, P. Dhull, R. D. Adams, M. V. Bobo, A. A. Vannucci, M. D. Smith, S. Garashchuk and N. B. Shustova, *Chem. Sci.*, 2021, **12**, 6600–6606.
36 Q. S. Stöckl, T. C. Wu, A. Mairena, Y. T. Wu and K. H. Ernst, *Faraday Discuss.*, 2017, **204**, 429–437.

37 Q. Xu, C. Wang, D. Zheng, J. He, Y. Wang, X. Chen and H. Jiang, *J. Org. Chem.*, DOI:10.1021/acs.joc.0c03065.
38 Q. Xu, C. Wang, J. He, X. Li, Y. Wang, X. Chen, D. Sun and H. Jiang, *Org. Chem. Front.*, 2021, **8**, 2970-2976.
39 H. A. Lin, K. Kato, Y. Segawa, L. T. Scott and K. Itami, *Chem. Sci.*, 2019, **10**, 2326–2330.
40 J. M. Fernández-García, P. J. Evans, S. Medina Rivero, I. Fernández, D. García-Fresnadillo, J. Perles, J. Casado and N. Martín, *J. Am. Chem. Soc.*, 2018, **140**, 17188–17196.
41 T. Wang, J. Lawrence, N. Sumi, R. Robles, J. Castro-Esteban, D. Rey, M. S. G. Mohammed, A. Berdonces-Layunta, N. Lorente, D. Pérez, D. Peña, M. Corso and D. G. de Oteyza, *Phys. Chem. Chem. Phys.*, 2021, **23**, 10845–10851.
42 K. Shoyama and F. Würthner, *J. Am. Chem. Soc.*, 2019, **141**, 13008–13012.
43 M. Qasemnazhand, F. Khoeini and F. Marsusi, *Sci. Rep.*, 2021, **11**, 2511.
44 M. Y. Li, Y. X. Zhao, Y. B. Han, K. Yuan, S. Nagase, M. Ehara and X. Zhao, *ACS Appl. Nano Mater.*, 2020, **3**, 547–554.
45 A. R. Khamatgalimov and V. I. Kovalenko, *Int. J. Mol. Sci.*, 2021, **22**, 3760.
46 Y. D. Song and Q. T. Wang, *J. Mol. Model.*, 2021, **27**, 1–11.
47 L. Wang, Y. L. Liu, S. H. Chen, D. He, Q. J. Li and M. S. Wang, *Phys. Chem. Chem. Phys.*, 2021, **23**, 405–414.
48 E. M. Muzammil, D. Halilovic and M. C. Stuparu, *Commun. Chem.*, 2019, **2**, 58.
49 V. Barát and M. C. Stuparu, *Chem. Asian J.*, 2021, 16, 20–29.
50 X. Li, F. Kang and M. Inagaki, *Small*, 2016, **12**, 3206–3223.
51 M. C. Stuparu, *Acc. Chem. Res.*, 2021, **54**, 2858–2870.
52 D. Lu, R. Tao and Z. Wang, *Front. Chem. Sci. Eng.* 2019, **13**, 310–323.
53 X. Q. Hou, Y. T. Sun, L. Liu, S. T. Wang, R. L. Geng and X. F. Shao, *Chinese Chem. Lett.*, 2016, **27**, 1166–1174.
54 D. R. Jones, P. Bachawala and J. Mack, *Top. Curr. Chem.*, 2014, **348**, 37–52.
55 C. B. Larsen and N. T. Lucas, *ChemInform*, 2012, **2**, 49–55.
56 M. A. Petrukhina and L. T. Scott, *Dalt. Trans.*, 2005, 2969–2975.
57 J. Li, A. Terec, W. Yue, H. Joshi, Y. Lu, H. Sun and M. C. Stuparu, *J. Am. Chem. Soc.*, 2017, **139**, 3089–3094.
58 H. Furukawa and O. M. Yaghi, *J. Am. Chem. Soc.*, 2009, **131**, 8875–8883.
59 K. T. Jackson, M. G. Rabbani, T. E. Reich and H. M. El-Kaderi, *Polym. Chem.*, 2011, **2**, 2775–2777.
60 A. Mishra, M. Ulaganathan, E. Edison, P. Borah, A. Mishra, S. Sreejith, S. Madhavi and M. C. Stuparu, *ACS Macro Lett.*, 2017, **6**, 1212–1216.
61 C. Bruno, R. Benassi, A. Passalacqua, F. Paolucci, C. Fontanesi, M. Marcaccio, E. A. Jackson and L. T. Scott, *J. Phys. Chem. B*, 2009, **113**, 1954–1962.
62 A. V. Zabula, A. S. Filatov, S. N. Spisak, A. Y. Rogachev and M. A. Petrukhina, *Science.*, 2011, **333**, 1008–1011.
63 S. N. Spisak, Z. Wei and M. A. Petrukhina, *Dalt. Trans.*, 2017, **46**, 5625–5630.
64 A. V. Zabula, S. N. Spisak, A. S. Filatov, A. Y. Rogachev and M. A. Petrukhina, *Acc. Chem. Res.*, 2018, **51**, 1541–1549.
65 M. A. Petrukhina, *Dalt. Trans.*, 2019, **48**, 5125–5130.
66 T. Eom, V. Barát, A. Khan and M. C. Stuparu, *Chem. Sci.*, 2021, **12**, 4949–4957.
67 X. Gu, X. Zhang, H. Ma, S. Jia, P. Zhang, Y. Zhao, Q. Liu, J. Wang, X. Zheng, J. W. Y. Lam, D. Ding and B. Z. Tang, *Adv. Mater.*, 2018, **30**, 1801065.
68 W. Lin, J. Gong, W. Ye, X. Huang and J. Chen, *Zeitschrift fur Anorg. und Allg. Chemie*, 2020, **646**, 1900–1903.
69 T. Hirao, K. Fukuta and T. Haino, *Macromolecules*, 2020, **53**, 3563–3570.
70 T. Hirao, Y. Iwabe, N. Fujii and T. Haino, *J. Am. Chem. Soc.*, 2021, **143**, 4339–4345.
71 D. E. Williams, E. A. Dolgopolova, D. C. Godfrey, E. D. Ermolaeva, P. J. Pellechia, A. B. Greytak, M. D. Smith, S. M. Avdoshenko, A. A. Popov and N. B. Shustova, *Angew. Chem. Int. Ed.*, 2016, **55**, 9070–9074.
72 D. Cui, M. Ebrahimi, F. Rosei and J. M. Macleod, *J. Am. Chem. Soc.*, 2017, **139**, 16732–16740.
73 D. Cui, J. M. MacLeod and F. Rosei, *Small*, 2019, **15**, 1903294.
74 J. Plas, O. Ivasenko, N. Martsinovich, M. Lackinger and S. De Feyter, *Chem. Commun.*, 2016, **52**, 68–71.
75 D. Cui, M. Ebrahimi, J. M. Macleod and F. Rosei, *Nano Lett.*, 2018, **18**, 7570–7575.
76 D. Bessinger, L. Ascherl, F. Auras and T. Bein, *J. Am. Chem. Soc.*, 2017, **139**, 12035–12042.
77 A. M. Rice, E. A. Dolgopolova, B. J. Yarbrough, G. A. Leith, C. R. Martin, K. S. Stephenson, R. A. Heugh, A. J. Brandt, D. A. Chen, S. G. Karakalos, M. D. Smith, K. B. Hatzell, P. J. Pellechia, S. Garashchuk and N. B. Shustova, *Angew. Chem. Int. Ed.*, 2018, **57**, 11310–11315.
78 G. A. Leith, A. M. Rice, B. J. Yarbrough, A. A. Berseneva, R. T. Ly, C. N. Buck, D. Chusov, A. J. Brandt, D. A. Chen, B. W. Lamm, M. Stefik, K. S. Stephenson, M. D. Smith, A. K. Vannucci, P. J. Pellechia, S. Garashchuk and N. B. Shustova, *Angew. Chem. Int. Ed.*, 2020, **59**, 6000–6006.
79 Y. Feng, X. Wang, P. Dong, J. Li, J. Huang, L. Cao, T. Wang and C. Wang, *Fullerenes, Nanotub. Carbon Nanostructures*, 2020, **28**, 353–360.
80 H. Meng, C. Zhao, Y. Li, M. Nie, C. Wang and T. Wang, *Nanoscale*, 2018, **10**, 3291–3298.
81 A. M. Rice, W. B. Fellows, E. A. Dolgopolova, A. B. Greytak, A. K. Vannucci, M. D. Smith, S. G. Karakalos, J. A. Krause, S. M. Avdoshenko, A. A. Popov and N. B. Shustova, *Angew. Chem. Int. Ed.*, 2017, **56**, 4525–4529.
82 X. Liu, M. Kozlowska, T. Okkali, D. Wagner, T. Higashino, G. Brenner-Weiß, S. M. Marschner, Z. Fu, Q. Zhang, H. Imahori, S. Bräse, W. Wenzel, C. Wöll and L. Heinke, *Angew. Chem. Int. Ed.*, 2019, **58**, 9590–9595.
83 V. Martinez, B. Karadeniz, N. Biliškov, I. Lončarić, S. Muratović, D. Žilić, S. M. Avdoshenko, M. Roslova, A. A. Popov and K. Užarević, *Chem. Mater.*, 2020, **32**, 10628–10640.
84 W. B. Fellows, A. M. Rice, D. E. Williams, E. A. Dolgopolova, A. K. Vannucci, P. J. Pellechia, M. D. Smith, J. A. Krause and N. B. Shustova, *Angew. Chem. Int. Ed.*, 2016, **55**, 2195–2199.
85 M. Souto, J. Calbo, S. Mañas-Valero, A. Walsh, G. M. Espallargas and C. J. Beltrán, *Beilstein J. Nanotechnol*, 2019, **10**, 1883–1893.
86 D. Y. Zheng, X. M. Zhou, S. Mutyala and X. C. Huang, *Chem. Eur. J.*, 2018, **24**, 19141–19145.
87 H. Li, M. R. Hill, R. Huang, C. Doblin, S. Lim, A. J. Hill, R. Babarao and P. Falcaro, *Chem. Commun.*, 2016, **52**, 5973–5976.
88 C. Liu, C. Wang, H. Wang, T. Wang and J. Jiang, *Eur. J. Inorg. Chem.*, 2019, **2019**, 4815–4819.
89 M. A. Gordillo, D. K. Panda and S. Saha, *ACS Appl. Mater. Interfaces*, 2019, **11**, 3196–3206.
90 T. Ohmura, A. Usuki, Y. Mukae, H. Motegi, S. Kajiya, M. Yamamoto, S. Senda, T. Matsumoto and K. Tatsumi, *Chem. Asian J.*, 2016, **11**, 700–704.
91 N. Huang, K. Wang, H. Drake, P. Cai, J. Pang, J. Li, S. Che, L. Huang, Q. Wang and H. C. Zhou, *J. Am. Chem. Soc.*, 2018, **140**, 6383–6390.
92 J. Cao, Y. Feng, S. Zhou, X. Sun, T. Wang, C. Wang and H. Li, *Dalt. Trans.*, 2016, **45**, 11272–11276.
93 M. Juríček, N. L. Strutt, J. C. Barnes, A. M. Butterfield, E. J. Dale, K. K. Baldridge, J. F. Stoddart and J. S. Siegel, *Nat. Chem.*, 2014, **6**, 222–228.
94 B. M. Schmidt, T. Osuga, T. Sawada, M. Hoshino and M. Fujita, *Angew. Chem. Int. Ed.*, 2016, **55**, 1561–1564.
95 H. Khuntia, K. S. Bhavani, T. Anusha, T. Trinadh, M. C. Stuparu

and P. K. Brahman, *Colloids Surfaces A Physicochem. Eng. Asp.*, 2021, **615**, 126237.
96 W. Sun, Y. Wang, L. Ma, L. Zheng, W. Fang, X. Chen and H. Jiang, *J. Org. Chem.*, 2018, **83**, 14667–14675.
97 T. Tsutsui, L. Catti, K. Yoza and M. Yoshizawa, *Chem. Sci.*, 2020, **11**, 8145–8150.
98 Y.-D. Yang, X.-L. Chen, J. L. Sessler and H.-Y. Gong, *J. Am. Chem. Soc.*, 2021, **143**, 2315–2324.
99 Y.-Y. Xu, H.-R. Tian, S.-H. Li, Z.-C. Chen, Y.-R. Yao, S.-S. Wang, X. Zhang, Z.-Z. Zhu, S.-L. Deng, Q. Zhang, S. Yang, S.-Y. Xie, R.-B. Huang and L.-S. Zheng, *Nat. Commun.*, 2019, **10**, 485.
100 R. Q. Lu, S. Wu, Y. H. Bao, L. L. Yang, H. Qu, M. Saha, X. Y. Wang, Y. Z. Zhuo, B. Xu, J. Pei, H. Zhang, W. Weng and X. Y. Cao, *Chem. Asian J.*, 2018, **13**, 2934–2938.
101 M. Madhu, R. Ramakrishnan, V. Vijay and M. Hariharan, *Chem. Rev.*, 2021, **121**, 8234−8284.
102 A. Kraft and F. Beuerle, *Tetrahedron Lett.*, 2016, **57**, 4651–4663.
103 S. Das and M. Presselt, *J. Mater. Chem. C*, 2019, **7**, 6194–6216.
104 F. Huang, L. Ma, Y. Che, H. Jiang, X. Chen and Y. Wang, *J. Org. Chem.*, 2018, **83**, 733–739.
105 A. Szumna, *Chem. Soc. Rev.*, 2010, **39**, 4274–4285.
106 Y.-D. Yang and H.-Y. Gong, *Chem. Commun.*, 2019, **55**, 3701–3704.
107 A. Sygula, F. R. Fronczek, R. Sygula, P. W. Rabideau and M. M. Olmstead, *J. Am. Chem. Soc.*, 2007, **129**, 3842–3843.
108 A. V. Zabula, Y. V. Sevryugina, S. N. Spisak, L. Kobryn, R. Sygula, A. Sygula and M. A. Petrukhina, *Chem. Commun.*, 2014, **50**, 2657–2659.
109 P. A. Denis and F. Iribarne, *Int. J. Quantum Chem.*, 2015, **115**, 1668–1672.
110 D. C. Yang, M. Li and C. F. Chen, *Chem. Commun.*, 2017, **53**, 9336–9339.
111 M. Takeda, S. Hiroto, H. Yokoi, S. Lee, D. Kim and H. Shinokubo, *J. Am. Chem. Soc.*, 2018, **140**, 6336–6342.
112 Y. Shoji, T. Kajitani, F. Ishiwari, Q. Ding, H. Sato, H. Anetai, T. Akutagawa, H. Sakurai and T. Fukushima, *Chem. Sci.*, 2017, **8**, 8405–8410.
113 Y. Haketa, M. Miyasue, Y. Kobayashi, R. Sato, Y. Shigeta, N. Yasuda, N. Tamai and H. Maeda, *J. Am. Chem. Soc.*, 2020, **142**, 16420–16428.
114 G. J. Moore, M. Causa', J. F. Martinez Hardigree, S. Karuthedath, I. Ramirez, A. Jungbluth, F. Laquai, M. Riede and N. Banerji, *J. Phys. Chem. Lett.*, 2020, **11**, 5610–5617.
115 Y. Wu, Y. Zhen, Z. Wang and H. Fu, *J. Phys. Chem. A*, 2013, **117**, 1712–1720.
116 X. Yu, B. Wang, Y. Kim, J. Park, S. Ghosh, B. Dhara, R. D. Mukhopadhyay, J. Koo, I. Kim, S. Kim, I. C. Hwang, S. Seki, D. M. Guldi, M. H. Baik and K. Kim, *J. Am. Chem. Soc.*, 2020, **142**, 12596–12601.
117 V. Leonhardt, S. Fimmel, A. M. Krause and F. Beuerle, *Chem. Sci.*, 2020, **11**, 8409–8415.
118 T. K. Ronson, Y. Wang, K. Baldridge, J. S. Siegel and J. R. Nitschke, *J. Am. Chem. Soc.*, 2020, **142**, 10267–10272.
119 C. Garciá-Simón, C. Colomban, Y. A. Çetin, A. Gimeno, M. Pujals, E. Ubasart, C. Fuertes-Espinosa, K. Asad, N. Chronakis, M. Costas, J. Jiménez-Barbero, F. Feixas and X. Ribas, *J. Am. Chem. Soc.*, 2020, **142**, 16051–16063.
120 F. Zhang, W. Shi, J. Luo, N. Pellet, C. Yi, X. Li, X. Zhao, T. J. S. Dennis, X. Li, S. Wang, Y. Xiao, S. M. Zakeeruddin, D. Bi and M. Grätzel, *Adv. Mater.*, 2017, **29**, 1606806.
121 R. Q. Lu, Y. Q. Zheng, Y. N. Zhou, X. Y. Yan, T. Lei, K. Shi, Y. Zhou, J. Pei, L. Zoppi, K. K. Baldridge, J. S. Siegel and X. Y. Cao, *J. Mater. Chem. A*, 2014, **2**, 20515–20519.
122 B. T. Muhammad, V. Barát, T. M. Koh, X. Wu, A. Surendran, N. Yantara, A. Bruno, A. C. Grimsdale, M. C. Stuparu and W. L. Leong, *Chem. Commun.*, 2020, **56**, 11997–12000.
123 S. Collavini and J. L. Delgado, *Sustain. Energy Fuels*, 2018, **2**, 2480–2493.
124 T. Umeyama and H. Imahori, *Acc. Chem. Res.*, 2019, **52**, 2046–2055.
125 N. Y. Doumon, M. V. Dryzhov, F. V. Houard, V. M. Le Corre, A. Rahimi Chatri, P. Christodoulis and L. J. A. Koster, *ACS Appl. Mater. Interfaces*, 2019, **11**, 8310–8318.
126 R. Renner, B. Mahlmeister, M. Stolte and F. Würthner, *Org. Mater.*, 2020, **2**, 229–234.

